Role of the C-Terminal Helix 9 in the Stability and Ligandin Function of Class α Glutathione Transferase A1-1[†]

Heini W. Dirr* and Louise A. Wallace

Protein Structure-Function Research Program, Department of Biochemistry, University of the Witwatersrand, Johannesburg 2050, South Africa

Received May 21, 1999; Revised Manuscript Received September 22, 1999

ABSTRACT: Helix 9 at the C-terminus of class α glutathione transferase (GST) polypeptides is a unique structural feature in the GST superfamily. It plays an important structural role in the catalytic cycle. Its contribution toward protein stability/folding as well as the binding of nonsubstrate ligands was investigated by protein engineering, conformational stability, enzyme activity, and ligand-binding methods. The helix9 sequence displays an unfavorable propensity toward helix formation, but tertiary interactions between the amphipathic helix and the GST seem to contribute sufficient stability to populate the helix on the surface of the protein. The helix's stability is enhanced further by the binding of ligands at the active site. The order of ligand-induced stabilization increases from H-site occupation, to G-site occupation, to the simultaneous occupation of H- and G-sites. Ligand-induced stabilization of helix9 reduces solvent accessible hydrophobic surface by facilitating firmer packing at the hydrophobic interface between helix and GST. This stabilized form exhibits enhanced affinity for the binding of nonsubstrate ligands to ligandin sites (i.e., noncatalytic binding sites). Although helix9 contributes very little toward the global stability of hGSTA1-1, its conformational dynamics have significant implications for the protein's equilibrium unfolding/refolding pathway and unfolding kinetics. Considering the high concentration of reduced glutathione in human cells (about 10 mM), the physiological form of hGSTA1-1 is most likely the thiol-complexed protein with a stabilized helix9. The C-terminus region (including helix9) of the class α polypeptide appears not to have been optimized for stability but rather for catalytic and ligandin function.

The supergene family of glutathione transferases (EC 2.5.1.18; GSTs) are represented by membrane-bound and soluble enzymes which function in the detoxification of alkylating agents, biosynthesis of physiologically important glutathione conjugates such as leukotriene A, and isomerization of steroids (*1*). Furthermore, the abundant and highly soluble cytosolic GSTs are implicated as binding/transport proteins for a wide variety of chemically diverse hydrophobic nonsubstrate ligands (*2*). Cytosolic GSTs are stable dimers ($M_r \approx 50\,000$) and can be grouped into six species-independent gene classes: α, μ, π (*3*), σ (*4*), θ (*5*), and κ (*6*). They share a highly conserved archetypical fold with a bi-domain subunit structure (reviewed in refs *7* and *8*), as illustrated in Figure 1 for the crystal structure of human class α GSTA1-1.[1] Stability studies have been performed on cytosolic GSTs from class α (*9*, *10*), class π (*11*−*14*), class σ (*15*), and a class μ Sj26GST (*16*), which is extensively used as an affinity tag in pGEX gene-fusion systems. The findings from these studies reflect the differences in conformational stability between the GST gene classes in that the Gibbs' free energies for partially folded intermediates range from extremely unfavorable to favorable. Each GST subunit has an active site situated predominantly on the thioredoxin-like domain (i.e., the N-terminus domain). The active site can be divided into two subsites: a polar site for binding the physiological tripeptide glutathione (G-site) and an adjacent hydrophobic region for electrophile substrates (H-site).

Class α GSTs have a unique structural feature in the form of an amphipathic α helix (helix9) at the C-terminus of the A1 polypeptide chain which can fold onto domain I (*17*, *18*) (Figure 1). This helix, although not essential for catalytic activity (*19*), is a structural determinant for specificity toward hydrophobic electrophiles. When packed onto domain I it becomes an integral part of the H-site providing a highly hydrophobic wall for the electrophile binding pocket and restricts accessibility of the H-site from bulk solvent. Furthermore, it has been suggested that the helix impacts on the ionization of Tyr8 in rat GSTA1-1 (*20*) a conserved catalytic residue involved in activating the thiol group of glutathione. The dynamic nature of helix9 in GSTA1-1 is evident from crystallographic (*17*, *18*) and NMR (*21*) data. In the protein uncomplexed with substrate/product, helix 9 is thought to be either disordered or structured, but conformationally highly mobile. In the complexes with substrate/

[†] This work was supported by the University of the Witwatersrand and the South African Foundation for Research Development. Partial support was received from the Alexander von Humboldt Stiftung for H.W.D. on sabbatical leave at EMBL, Heidelberg, Germany.

* To whom correspondence should be addressed. E-mail: 089dirr@cosmos.wits.ac.za. Fax: +27 11 403 1733. Phone: +27 11 716 2265.

[1] Abbreviations: a9del, helix9 deletion; AEDANS, 5-[[2-(acetylamino)ethyl]amino]naphthalene-1-sulfonic acid; ANS, anilinonaphthalene sulphonate; BSP, bromosulphophthalene; C_m, concentration of denaturant at midpoint of unfolding transition; G- and H-sites, glutathione and hydrophobic sites; hGSTA1-1, human glutathione transferase class α with two type-1 subunits; HPLC, high-performance liquid chromatography; NMR, nuclear magnetic resonance; *m*-value, dependence of Gibbs free energy of unfolding on denaturant concentration; Sj26GST, *Schistosoma japonica* glutathione transferase with 26 kDa subunits; UV, ultraviolet.

10.1021/bi991179x CCC: $18.00
Published on Web 11/03/1999

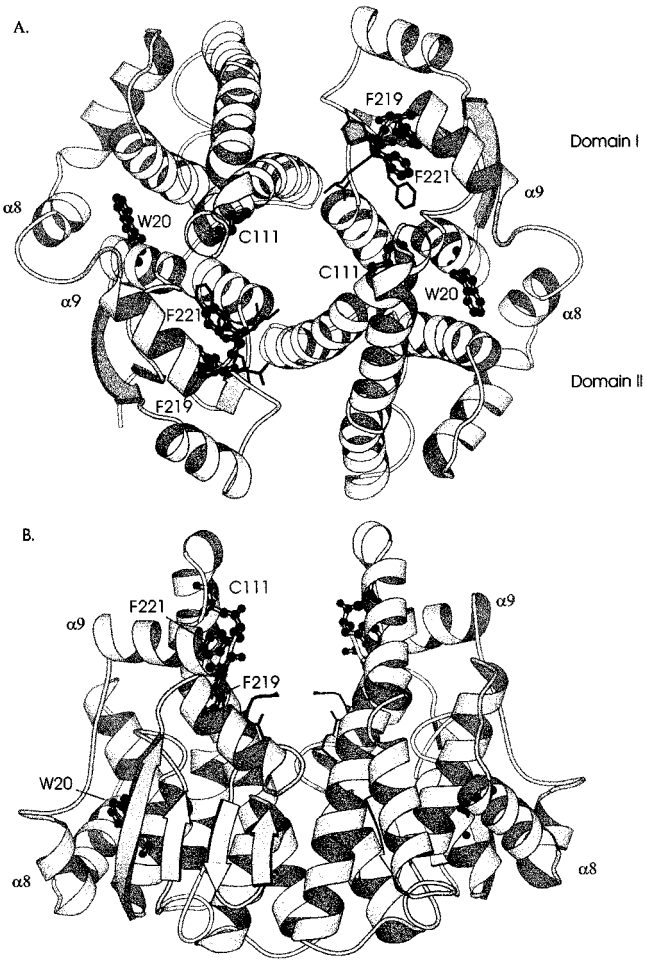

FIGURE 1: Ribbon representation of human class α GSTA1-1 (*17*), down (A) and perpendicular (B) to the dimer 2-fold axis. The locations of helix8 (α8) at the domain−domain interface and helix9 (α9) above domain I are shown. The side chains of Trp20, Cys111, Phe219, and Phe221 are shown as ball-and-stick representations. The active site ligand *S*-benzylglutathione is shown in bold. The diagrams were generated by MOLSCRIPT (*46*).

product, the helix becomes stabilized and its position on domain I better defined but remains to exhibit above-average temperature factors.

Dimerization of GST subunits results in the formation of a nonsubstrate ligand-binding region within the solvent filled amphipathic cleft between the subunits (*22*−*26*). Topographically, this cleft, which runs along the subunit interface from one active site to the other, ranges from wide and open to solvent (class α) to narrow and restricted (class σ). The C-terminal end of helix9 in GSTA1-1 is located next to the cleft (Figure 1). Because of the restricted topography of the H-site in class α GSTs (due to the presence of helix9), the solvent-accessible cleft may also be utilized to some extent by the enzyme to accommodate the larger electrophile substrates (*17*, *18*).

Very little is known about the role of helix9 in determining protein stability and the binding of nonsubstrate ligands to class α GSTs. In this study, we investigate the role of helix 9 in the stability of hGSTA1-1 as well as in the protein's ligandin function by using wild-type hGSTA1-1, a deletion mutant (a9del) in which residues 210−221 (including those for helix 9; i.e., 210−219) have been truncated, and a F219W mutant.

EXPERIMENTAL PROCEDURES

Materials. Human GSTA1-1 was overexpressed from the plasmid pKHA1 [a gift from Prof. Mannervik (*27*)] in *Escherichia coli* JM 103 cells (*9*, *10*). Site-directed mutagenesis was performed by combining inverse PCR with long PCR to introduce the mutation directly into an intact plasmid template (ref *28*; Ex-site mutagenesis kit from Stratagene). The oligonucleotides used for deletion of helix 9 (a9del GSTA1-1; residues 210−221) were 5′TAATCTCTAGAAGAAGCAAGGAAG3′ and 5′CTCATCCATGGGAGGCTTCC3′. The underlined nucleotides represent the stop codon at position 210 (after Glu209). The oligonucleotides used for introduction of tryptophan at position 219 (F219W GSTA1-1) were 5′CCTTGCTTCTTCTAAAGATTT3′ and 5′AAGATCTGGAGGTTTTAATAACGCAGTCAT3′. The underlined nucleotides represent the mutation that generates the Phe to Trp substitution. Translationally silent mutations incorporating unique restriction sites were used to screen for the mutant plasmids. The entire cDNA encoding the mutant GSTA1-1 was sequenced to ensure that no other mutations were introduced into the nucleotide sequence during PCR. GSTA1-1 was purified using *S*-hexylglutathione affinity chromatography (*18*, *27*) and eluted as previously described (*9*). Because of the reduced affinity of a9del GSTA1-1 and F219W GSTA1-1 for the *S*-hexylglutathione affinity matrix, the proteins were purified using CM-Sephadex cation-exchange chromatography. The column was preequilibrated with 10 mM sodium phosphate buffer, pH 7.0, and the protein eluted using a 0 to 0.5 M NaCl gradient. The mutant proteins eluted at approximately 0.3 M NaCl and the GST-containing samples were buffer-exchanged into 20 mM sodium phosphate buffer, pH 6.5, containing 0.1 M NaCl and 1 mM EDTA. The purity of the wild-type and mutant proteins as judged by SDS−PAGE (*29*) and SEC−HPLC was greater than 95%. The protein concentration of dimeric wild-type and a9del GSTA1-1 was estimated spectrophotometrically using a molar extinction coefficient of 38 200 M^{-1} cm^{-1} at 280 nm, calculated using the method described by Perkins (*30*). The protein concentration of dimeric F220W GST A1−1 was estimated spectrophotometrically using a molar extinction coefficient of 49 300 M^{-1} cm^{-1} at 280 nm. Ultrapure urea was from ICN Biomedicals. All other reagents were of analytical grade.

Enzyme Activity and Ligand Binding. Enzyme activity was determined spectrophotometrically at 340 nm in 0.1 M sodium phosphate buffer, pH 6.5, containing 1 mM glutathione and 1 mM chloro-2,4-dinitrobenzene. The interaction between GSTA1-1 and various ligands was determined by fluorescence quenching and enhancement methods (*31*). Fluorescence resonance energy transfer measurements between Trp20 in GSTA1-1 and bound ANS as well as the analysis of the data were performed as described (*24*, *25*).

Acrylamide Quenching. The exposure to solvent of Trp20 in wild-type and mutant GSTA1-1 was determined by a Stern−Volmer analysis of quenching data at low (0−0.15 M) concentrations of acrylamide (*11*).

Circular Dichroism. Circular dichroism measurements were made in a Jasco J-710 spectropolarimeter, with a path length of 1 mm. Spectra are an average of 16 runs.

Unfolding Studies. Equilibrium unfolding/refolding and reversibility experiments were performed as described (*9*,

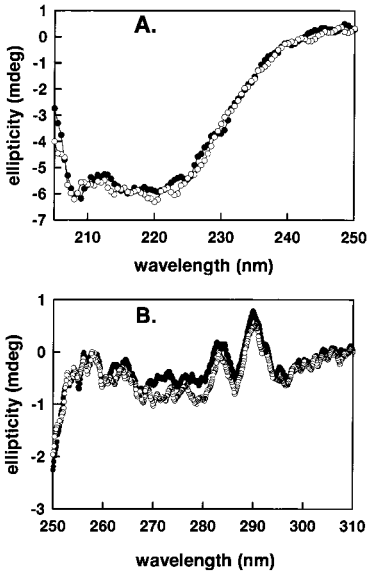

FIGURE 2: Far-UV (A) and near-UV (B) circular dichroism spectra for wild-type (●) and a9del (○) human GSTA1-1. Protein concentration was 1 and 10 μM for far-UV and near-UV, respectively, in 20 mM sodium phosphate, pH 6.5, containing 0.1 M NaCl.

10) at 25 °C in 20 mM sodium phosphate buffer, pH 6.5, containing 1 mM EDTA and 0.1 M NaCl. Unfolding kinetics were followed by stopped-flow in an Applied Photophysics SX-18MV apparatus as reported (*9*, *10*). Far-UV circular dichroism measurements at 226 nm were carried out using the Applied Photophysics circular dichroism kinetic accessory (CD.2C) interfaced to the stopped-flow apparatus. A path length of 2 mm and slits widths of 0.5 mm and 1 mm for monochromator 1 and 2, respectively, were used. Calibration was done with (1S)-(+)-10-camphorsulfonic acid. The dead-time for circular dichroism was 10 ms according to the method of Tonomura et al. (*32*). All kinetic traces were analyzed with the Applied Photophysics software v.4.24/4.36.

AGADIR Calculations. The predicted helix content of amino acid sequences was calculated using the AGADIR1s-2 algorithm (*33*) available via a Web-based interface at http://www.embl-heidelberg.de/Services/index.html#5. Conditions used were temperature, 295 K; pH 6.5; and ionic strength, 0.1 M.

RESULTS

Characterization of Wild-Type hGSTA1-1 and the a9del and F219W Mutants. The far-UV circular dichroism spectra for hGSTA1-1 (Figure 2A) indicate that the truncation of the C-terminus region (residues 210−221) does not impact on the secondary structure of the protein. Spectra displaying two ellipticity minima at 222 and 208 nm are typical for a protein with a high α-helix content (*34*). According to the crystal structures for hGSTA1-1 (*17*, *18*), about 60% of all amino acid residues are in α-helices and about 10% in β-strands. Helix9 (residues 210−219) in the C-terminus region contributes 4.5% points toward the total helix content. This low percentage does not allow circular dichroism to differentiate between the wild-type and a9del GSTA1-1. The near-UV circular dichroism spectra for wild-type and a9del proteins (Figure 2B) indicate similar but not identical packing environments for Trp20 in the two proteins.

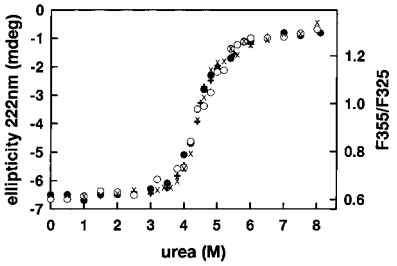

FIGURE 3: Urea-induced equilibrium unfolding curves for 1 μM wild-type and a9del hGSTA1-1 monitored by Trp20 fluorescence (X, wild-type; +, a9del) and ellipticity at 222 nm (○, wild-type; ●, a9del). F355/F325 is the ratio of the fluorescence intensity at 355 nm to that at 325 nm and represents the degree of exposure of Trp20 to solvent.

Each subunit of hGSTA1-1 has a single tryptophan residue (Trp20), which is located at the domain−domain interface (Figure 1). Its indole side chain extends from helix1 of domain I into a tertiary environment in domain II formed by Ile157, Glu161, and Tyr164 in helix6 and Phe196, Leu197 at the C-terminus of helix8. The conformation and environment of Trp20 in hGSTA1-1 are essentially the same for the uncomplexed and ligand-complexed enzyme (*17*, *18*). An identical emission maximum of 325 nm for uncomplexed/complexed enzyme indicates that the polarity of their Trp20 environments are very similar. However, the emission maximum for Trp20 is shifted from 325 to 330 nm in the helix9-truncated enzyme indicative of an increased exposure of Trp20 to solvent. This red-shift in wavelength was accompanied by a 20% enhancement in emission intensity which could be the consequence of the indole side chain moving away from the potential quenching effect of Glu161 due to looser packing of helix8 at the domain interface. Steady-state anisotropy studies indicate Trp20 to be slightly more mobile in the a9del protein (anisotropy 0.079) than in wild-type hGSTA1-1 (anisotropy 0.09). The value for the unfolded protein is 0.04. These and the near-UV circular dichroism data above suggest a less tightly packed Trp20 in the a9del mutant. The fluorescence emission maximum for the F219W mutant is at 325 nm, and the additional tryptophan residue at position 219 contributes only 23% toward the total emission intensity. This indicates that Trp20 is the dominant fluorophore in the mutant. The emission spectrum for Trp219 in the mutant (obtained from the difference between the emission spectra for wild-type and F219W; data not shown) has a maximum at 330 nm, indicating that its environment is more polar than that of Trp20.

In terms of catalytic function, the removal of helix9 and the replacement of Phe219 with a tryptophan residue are highly disruptive. The specific activity of a9del hGSTA1-1 is less than 1% of the wild-type value, demonstrating the significance of the C-terminus region in catalytic function. This is in agreement with the findings with class α enzyme GSTA2−2 (*19*). The activity was not increased by increasing the GSH concentration. Similar K_d values of 0.27 mM for wild-type and 0.35 mM for a9del mutant suggest that the effect was not due to a lack of occupation at the G-site by GSH. The specific activity of the F219W mutant is about 6% of the wild-type value.

Equilibrium Unfolding/Refolding. Urea-induced unfolding transitions are shown in Figure 3. Trp20 fluorescence and

222 nm ellipticity data are coincident and follow a single sigmoidal transition. Furthermore, similar T_m values at about 60 °C were obtained for both proteins during thermal unfolding while monitoring the disappearance of ellipticity at 222 nm with increasing temperature (data not shown). The urea-induced unfolding transition for the F219W mutant also resembles those observed for wild-type/a9del GSTA1-1 (data not shown). Unlike the fluorescence intensity of Trp20, the fluorescence intensity for Trp219 increases about 13% from 0 to 4 M urea, which precedes the major (global) unfolding transition of the protein (data not shown). The similar thermodynamic stabilities observed for the wild-type and mutant proteins is consistent with a negligible mutation-induced change in the core structure of the protein. This was substantiated by their similar hydrodynamic volumes (as determined by size-exclusion HPLC; data not shown) and secondary structures (see above). Thermodynamic parameters obtained from the unfolding data are midpoint of transition curve (C_m) = 4.6 M urea; difference in Gibbs' free energy between folded and unfolded protein [i.e., $\Delta G(H_2O)$] = 27.6 kcal/mol for wild-type and 25.2 kcal/mol for a9del; dependence of ÄG of unfolding on denaturant concentration (*m* value) = 4.2 kcal/mol/M urea for wild-type and 3.8 kcal/mol/M for a9del. The predicted *m* values for wild-type and a9del hGSTA1-1, based on their sizes (i.e., 221 and 209 residues, respectively) are 4.8 and 4.6 kcal/mol/M urea [according to Myers et al. (*35*)].

For wild-type protein, the enzyme activity transition is not coincident with the structural spectroscopic data; loss in enzyme activity occurs at lower urea concentrations (transition midpoints at 3.8 M for activity and 4.6 M for the fluorescence/222 nm ellipticity data; Figures 3 and 4A). The pretransition baselines for the fluorescence and 222 nm ellipticity data show very little if any dependence upon urea concentration. The pretransition for enzyme activity, however, is urea dependent, displaying a decrease in activity prior to the major activity transition; about 20−25% deactivation occurs at 3−3.5 M urea. Due to the low specific activities of the mutants, it was not possible to use enzyme activity to probe their unfolding. The hydrodynamic volume of hGSTA1-1 and fluorescence emission maximum did not change with urea up to 3.5M.

Effect of Active-Site Ligands on Stability. The effect of ligand binding to the active site on protein stability was investigated by complexing hGSTA1-1 with glutathione (K_d 0.27 mM) or the product analogue *p*-bromobenzyl glutathione (K_d 45 μM) prior to urea-induced denaturation. The unfolding curves shown in Figure 4B indicate that glutathione does not shift the position of the fluorescence transition (midpoint remains at 4.6 M urea) whereas *p*-bromobenzylglutathione shifts it toward slightly higher urea concentrations (midpoint shifts to 4.8 M urea; Figure 4C). The enzyme activity transition, however, is shifted to higher concentrations by both glutathione and *p*-bromobenzylglutathione; i.e., midpoint is shifted from 3.8M urea in absence of ligand to 4.3M urea for glutathione and 4.6 M urea for *p*-bromobenzylglutathione. It is interesting to note that the enzyme activity pretransition baselines have become essentially independent of urea concentration as compared with the baseline in the absence of ligand (Figure 4).

ANS Binding. The anionic dye ANS can be used to monitor the appearance/disappearance of hydrophobic surfaces on proteins undergoing structural changes (*36*). In this regard, ANS has been used successfully to follow the unfolding/refolding of GSTs (*9*, *12*, *15*). ANS itself does not impact on the stability of hGSTA1-1 (*9*), suggesting that the dye does not change the protein's conformation [e.g., by functioning as a conformational tightening agent as shown for some acid-expanded proteins (*47*)]. When ANS binds hGSTA1-1, its fluorescence is enhanced accompanied by a blue-shift in its emission maximum from 530 nm (free ANS in buffer) to 480 nm for wild-type protein or to 475 nm for the a9del and F219W mutants. When compared with the wild-type, both of the hGSTA1-1 mutants appear to exhibit a greater capacity to bind ANS as suggested by the 2.8- and 2-fold enhanced ANS fluorescence intensity for a9del and F219W, respectively. The affinity of a9del for ANS (K_d 10 μM) is about 3-fold stronger when compared with the wild-type (K_d 31 μM). The lower emission wavelength for ANS bound to the mutant proteins suggests a more nonpolar ANS-binding environment. Figure 5 illustrates the effect of urea on the binding of ANS to wild-type hGSTA1-1 and the a9del and F219W mutants in the absence and presence of active site ligands. Figure 5A shows that uncomplexed hGSTA1-1 exhibits increasing ANS binding between 1 and 4 M urea [i.e., within the region corresponding to the initial urea-induced deactivation of hGSTA1-1 (Figure 4A) and the fluorescence pre-transition baseline shown in Figure 3]. ANS binding then diminishes as the protein unfolds beyond 4 M urea. The enhanced ANS binding behavior is nearly abol-

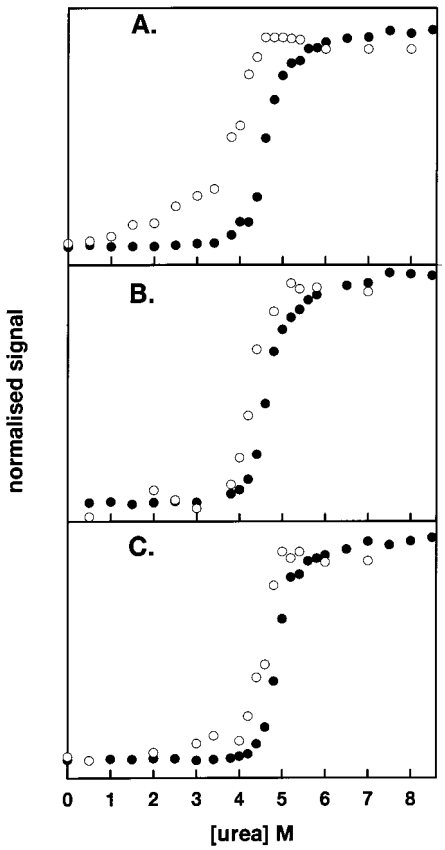

FIGURE 4: Urea-induced unfolding curves for 1 μM wild-type hGSTA1-1 in the absence (A) and presence of 10 mM glutathione (B) and 200 μM *p*-bromobenzylglutathione (C). (●) Trp20 fluorescence (i.e., F355/F325; see Figure 3) and (○) the loss of enzyme activity. The normalized signals represent an increasing fraction (0−1) of unfolded protein with increasing urea concentration.

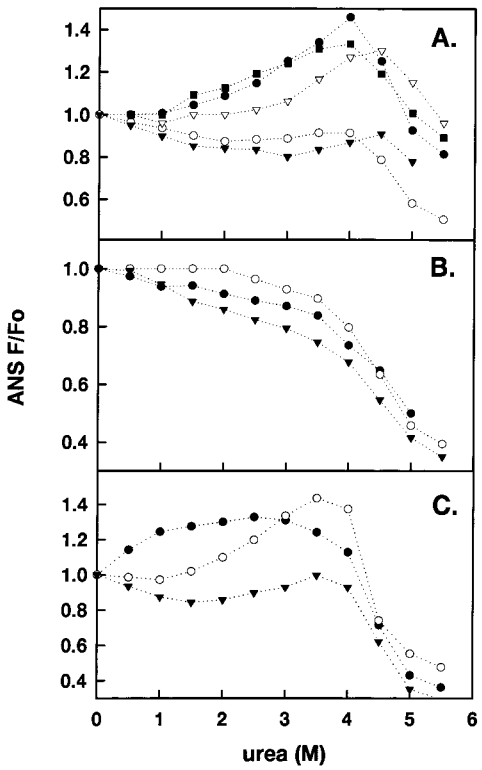

FIGURE 5: The effect of urea on the ability of wild-type (A), a9del (B), and F219W (C) hGSTA1-1 to bind the amphipathic dye ANS. Measurements of ANS fluorescence at 475 nm (excitation at 390 nm) were made in the absence (●) and presence of various ligands: 10 mM glutathione (○), 200 μM *p*-bromobenzylglutathione (▼), 2 mM ethacrynic acid (▽), and 100 μM BSP (■). Conditions were 1 μM protein dimer and 100 μM ANS in 20 mM sodium phosphate buffer, pH6.5, containing 0.1M NaCl. F/F_o is the ratio of ANS fluorescence at 475 nm in the presence and absence of ligand.

ished when the active site is occupied by either reduced glutathione or *p*-bromobenzylglutathione but less so by ethacrynic acid (Figure 5A). ANS binding diminishes beyond 4 M urea with glutathione and beyond 4.5 M urea with *p*-bromobenzylglutathione and ethacrynic acid. Unlike uncomplexed wild-type hGSTA1-1, the a9del protein does not exhibit urea-induced enhanced ANS binding behavior without/with glutathione or *p*-bromobenzylglutathione (Figure 5B). The unfolding pretransition for a9del protein resembles those observed for wild-type complexed with glutathione and *p*-bromobenzylglutathione. The constant decrease in ANS emission intensity with low urea concentrations may reflect competitive displacement of ANS from protein by urea (*37*). Figure 5C shows the F219W mutant to bind ANS at lower urea concentrations than those compared with wild-type. The presence of either glutathione or *p*-bromobenzylglutathione inhibit ANS binding at lower urea concentrations but not at higher denaturant concentrations. ANS binding diminishes beyond 4 M urea as the F219W mutant protein unfolds.

In addition to using ANS to probe hydrophobic surfaces during urea-induced structural changes, the dye can also be used to probe the behavior of a nonsubstrate ligand binding site of wild-type hGSTA1-1 in the absence of urea. Wild-type hGSTA1-1 binds ANS at a site located at the dimer interface (*23*). Its ability to bind ANS is improved when its active sites are occupied by glutathione or *p*-bromobenzylglutathione (Figure 6). No effect on ANS binding was

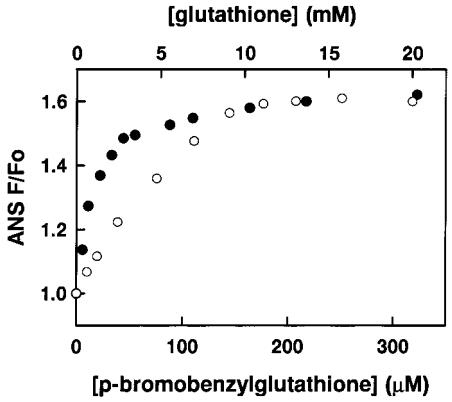

FIGURE 6: The effect of the active site ligands glutathione (○) and *p*-bromobenzylglutathione (●) on the binding of ANS to wild-type hGSTA1-1. Conditions were 1 μM protein dimer and 100 μM ANS in 20 mM sodium phosphate buffer, pH 6.5, containing 0.1M NaCl. ANS fluorescence was measured at 475 nm (excitation at 390 nm). F/F_o is the ratio of ANS fluorescence in the presence and absence of ligand.

observed with ethacrynic acid. Furthermore, the bound dye's emission maximum shifts from 480 to 473 nm, indicating that the polarity of the binding site has become more hydrophobic when glutathione/analogue is bound at the active site. A fluorescence resonance energy transfer study of ANS binding to hGSTA1-1 indicates that the efficiency of energy transfer between Trp20 and bound ANS to be similar without glutathione (efficiency = 30%) and with 10 mM glutathione (efficiency = 26%). This indicates that ANS binds the same region in uncomplexed and complexed protein [i.e., the amphiphilic cleft at the dimer interface (*24*, *25*)]. The affinity for ANS, however, was enhanced about 3-fold in the presence of 10 mM glutathione (i.e., K_d values of 31 and 10 μM without and with 10 mM glutathione, respectively). Glutathione has been shown not to have an effect on the binding of ANS to class sigma GSTS1-1 (*15*).

BSP Binding. BSP, which binds a site distinct from the ANS site (*24*, *25*, *31*), does not impact on the urea-dependent behavior of ANS binding to wild-type hGSTA1-1 (Figure 5A). Urea did not impact significantly on BSP's ability to bind GSTA1-1; K_d-values are 53 and 62 μM in the absence and presence of 4 M urea, respectively, with corresponding maximum quenching values of 68 and 74%. The fluorescence of Trp20 is quenched substantially by BSP (about 70%) in agreement with the proximity of its binding site to the fluorophore (*23*). The ability of hGSTA1-1 to bind BSP is enhanced about 3.5-fold when the G-site is occupied by glutathione (K_d decreases from 53 to 15 μM in the presence of 10 mM glutathione). Maximum quenching remained at about 70%. The a9del mutant displays a 2-fold higher affinity for BSP (K_d 25 μM) accompanied by an almost 100% quenching efficiency of Trp20 fluorescence. This is in agreement with a more solvent-exposed Trp20 in the mutant (see above and below).

Acrylamide Quenching. The exposure of Trp20 to solvent was determined by its ability to be quenched by the neutral and polar quencher acrylamide. From Stern−Volmer plots at low acrylamide concentrations (0−0.15 M) (data not shown; see ref *11*), values for the Stern−Volmer quenching constant, K_{sv}, for wild-type protein in the absence and presence of urea were estimated to be 3.2 M^{-1} (0 M urea), 4.2 M^{-1} (3 M urea), 4.4 M^{-1} (3.5 M urea), and 6.7 M^{-1} (4

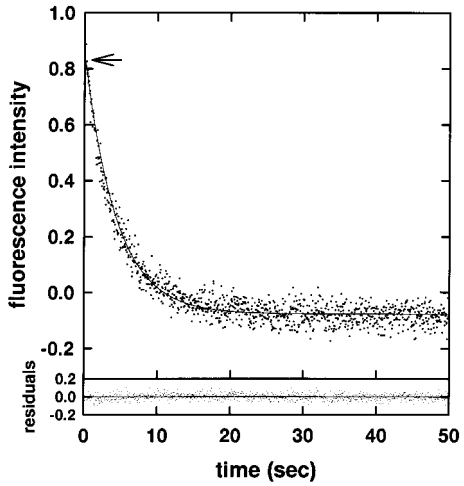

FIGURE 7: Unfolding kinetics of a9del hGSTA1-1. The change in fluorescence intensity of 1 μM protein was measured at 8.3M urea, pH6.5, 25 °C (excitation at 280 nm and emission at >320 nm). The arrow marks the position of the fluorescence signal for native folded protein indicating the absence of a burst phase. The trace was fitted to a single-exponential function. The lower panel shows the residuals for the fitted curve.

M urea). The corresponding values for the a9del mutant are 6.3 M^{-1} (0 M urea), 6.1 M^{-1} (3 M urea), 7.3 M^{-1} (3.5 M urea), and 8.4 M^{-1} (4 M urea). Static quenching (i.e., upward curving plots), were observed form the mutant at all urea concentrations and only at 4 M urea for wild-type. The data suggest that the exposure of Trp20 in wild-type GSTA1-1 to solvent is not much affected by urea up to 3.5 M and that the solvent accessibility of Trp20 is greater in the a9del mutant protein. The extent to which Trp20 in wild-type hGSTA1-1 becomes exposed to solvent at 4 M urea is similar to the exposure of Trp20 in the a9del mutant in the absence of urea (based on similar K_{sv} values).

Unfolding Kinetics. Figure 7 shows an unfolding kinetics trace for the a9del mutant monitored by tryptophan fluorescence. The trace is characterized by a monoexponential decrease in fluorescence (rate constant of 0.23 s^{-1}) and accounts for all of the total amplitude change. The rate constant is similar to those obtained for the slow unfolding phase of wild-type enzyme under similar conditions (i.e., 8.3 M urea) (*9*); i.e., 0.24 s^{-1} for Trp20 fluorescence and circular dichroism ellipticity at 226 nm, and 0.29 s^{-1} for AEDANS-labeled enzyme. The single unfolding phase for a9del displayed urea-dependence properties similar to those observed for the slow unfolding phase for wild-type hGSTA1-1 (*9*). The m_u values [i.e., the slope for log k_u versus urea concentration plots, which is related to the solvent accessible surface of the transition state (*38*); see Figure 4 in (*9*)] obtained for a9del by monitoring unfolding with Trp20 fluorescence (m_u = 218 cal/mol/M; r^2 = 0.990) and by circular dichroism ellipticity at 226 nm (m_u = 211.3 cal/mol/M urea; r^2 = 0.970) correspond very well with one another. The values for wild-type (*9*) are 270 cal/mol/M (r^2 = 0.992) for Trp fluorescence, 286.2 cal/mol/M (r^2 = 0.982) for AEDANS fluorescence, and 281.3 cal/mol/M (r^2 = 0.988) for circular dichroism. An indication of the position of the transition state for unfolding (in terms of its solvent accessibility) along the reaction coordinate can be estimated by dividing the kinetics m_u values with the equilibrium m values; m_u/m values for wild-type are 6.4, 6.8, and 6.7% for Trp fluorescence, AEDANS fluorescence and circular dichroism, respectively. The values for a9del are 5.8 and 5.6% for Trp fluorescence and circular dichroism, respectively. The solvent-accessible surface of the transition state for a9del GSTA1-1, therefore, closely resembles that for the native protein.

DISCUSSION

α-Helix 9 at the C-terminus of class α GST polypeptides is a unique structural feature in the GST family, and it plays an important structural role in the enzyme's catalytic cycle (*17*−*19*). However, the contribution of this helix toward protein stability and folding as well as the binding of nonsubstrate ligands is not known.

Intrinsic Stability of Helix9. Clear electron density for helix9 is observed in hGSTA1-1 only when the protein is complexed with active-site ligands (*17*, *18*). An intriguing question is whether helix9 is formed only when there is bound ligand or whether the helix is present but that its poor and uninterpretable electron density in uncomplexed protein is due to the high mobility of the helix. Application of the AGADIR algorithm (*32*) to the peptide sequence of helix9 in hGSTA1-1 gave us some insight about the intrinsic stability of this helix (i.e., the helix-forming tendency of the peptide sequence in the absence of tertiary interactions). A helix content of 11.4% was calculated, indicating a very low predicted population of helical conformers for the peptide. Therefore, helix9 would appear not to be able to fold independently of the rest of the protein. Recent hydrostatic pressure (*20*) and NMR (*21*) studies suggest that helix9 might not be completely unfolded/disordered in the uncomplexed protein. Rather, it may be intact but mobile and present as various isoenergetic conformations that differ in their degrees of solvation and packing against the protein. Crystallographic data do not seem to totally discount the presence of a mobile helix9 (rather than disordered helix9) since traces of electron density occur in uncomplexed enzyme at the expected position of the helix backbone (*18*). This is in support for a preexisting helix9 rather than a ligand-induced formation of helix9. It is apparent that data are not clear about the conformational state of the C-terminus region. Recently (*48*), the C-terminus in rat GSTA1-1 has been reported to undergo a ligand-dependent coil−helix transition and that there is evidence for a denatured state for the peptide.

Figure 8 illustrates the tertiary interactions between helix9 and the rest of the GST in the crystal structure of hGSTA1-1 complexed with *S*-benzylglutathione (*17*). Helix9 is amphipathic in nature, and its packing against the GST is mediated predominantly via hydrophobic interactions between residues in the hydrophobic face of the helix and residues in domain I and domain II. In the structure with *S*-benzylglutathione, there are 42 potential van der Waals contacts within 4A (including a salt bridge between Arg220 and Asp41). However, the number of potential contacts is diminished to 38 and 20 for the complexes with ethacrynic acid and glutathione−ethacrynic acid conjugate, respectively (*18*), with no salt bridge being present between Arg220 and Asp41 in both complexes. The Arg220−Asp41 ionic interaction is, therefore, not conserved in class α GSTs as suggested by others (*39*, *40*), but its formation is dependent on the nature of the ligand bound at the active site. A negatively charged Glu209 near the N-terminus and a positively charged Arg220

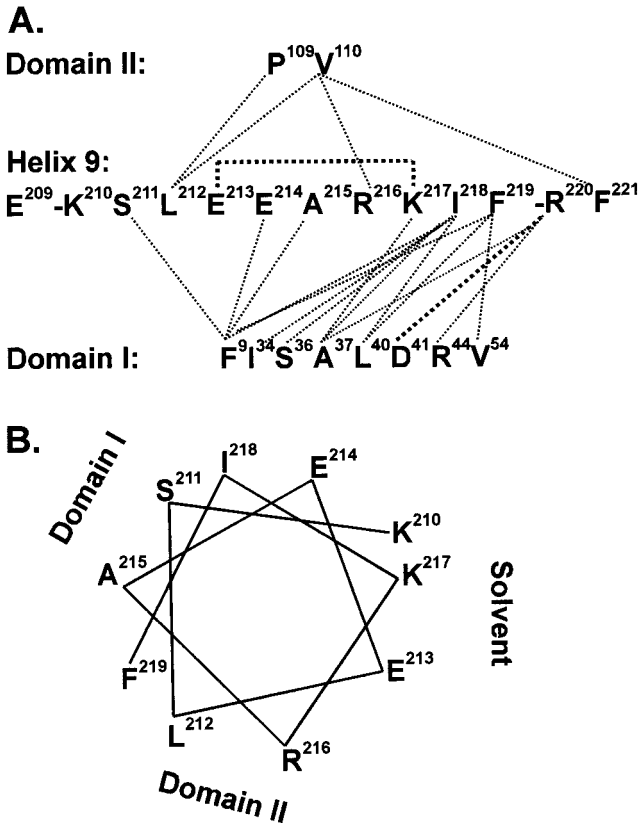

FIGURE 8: (A) schematic diagram to indicate the intrahelical (*i*,*i*+4) ion pair interaction (- − -) between E213 and K217 as well as the tertiary contacts (⋯) between helix9 and residues in domains I and II of hGSTA1-1 (*17*). In addition to the sequence for helix9 (K210−F219), E209 at the N-terminal end and R220 and F221 at the C-terminal end of the helix are also shown. The salt bridge between R220 and D41 is represented in bold. (B) A helical wheel projection of helix9 illustrating the positions of the residues with respect to domains I and II and the solvent. Residues K210, E213, E214, R216, and K217 are at the hydrophilic/solvent exposed face of helix9.

near the C-terminus of helix9 could function in charge-helix dipole interactions to stabilize the helix (*41*). Furthermore, an (*i*,*i*+4) side-chain ion pair interaction between Glu213 and Lys217 could also exert a stabilizing effect on the helix in the complex with *S*-benzylglutathione. This ion pair interaction is not seen in the complexes with ethacrynic acid or its glutathione conjugate. In addition to local/tertiary interactions, the only contacts within 4 Å between *S*-benzylglutathione bound at the active site of hGSTA1-1 and helix9 are those between the side chain of Phe219 and the cysteinyl and glycine moieties of the ligand (it seems likely that similar interactions would occur between reduced glutathione and Phe219). Phe219 does not make contact with the inhibitor's benzyl ring whereas Met207 and Phe 221 near the C- and N-terminal ends of helix9, respectively, do. In the complex with ethacrynic acid, in which the inhibitor binds in a nonproductive manner at the H-site with partial occupation of the free G-site (*18*), the ligand makes contacts with Phe219 as well as with Met207 and Phe221.

Helix9 and Conformational Stability of hGSTA1-1. In this study, uncomplexed wild-type hGSTA1-1 and the a9del and F219W mutants are shown to display similar overall stabilities toward urea and temperature denaturation, suggesting a minor contribution by helix9 toward the overall stability of the protein (as measured by fluorescence and 222 nm ellipticity). This finding is consistent with the two-state model previously proposed for the equilibrium unfolding/refolding of hGSTA1-1 involving native dimer and two unfolded monomers ($N_2 \leftrightarrow 2U$) (*9*, *10*). However, when catalytic activity is monitored, urea-dependent enzyme deactivation is observed not to coincide with the structural unfolding/refolding transition (Figure 3). This highlights the insensitivity of the spectroscopic probes toward structural changes occurring at low urea concentrations which impact significantly upon the enzyme's catalytic function. The initial loss of activity is accompanied by increased exposure of hydrophobic surface on the folded protein as indicated by enhanced ANS binding (Figure 5). Bound ANS is released from the protein beyond 4 M urea as a result of binding surfaces becoming disrupted during the global unfolding of the protein. The a9del hGSTA1-1, like the class pi GSTP1-1 (*12*) and class μ Sj26GST (*16*) which also do not have a helix9 equivalent, does not display increased ANS-binding behavior with increasing urea concentrations. That the absence of helix9 packed against domain I of GSTA1-1 results in the exposure of hydrophobic surface is indicated by the enhanced binding of ANS by the a9del mutant in the absence of urea. Helix9 in the F219W mutant appears to be more susceptible to urea-induced structural changes resulting in the exposure of hydrophobic surface at lower urea concentrations than those seen with wild-type protein. The weaker association of helix9 with domain I of the F219W mutant in the absence of urea is suggested by the enhanced binding of ANS to the mutant. Phe219 is conserved in class α and is proposed to modulate the stability of the helix via interactions with residues in domain I (*18*); its phenyl side chain fits into a hydrophobic pocket formed by the side chains of Tyr8, Phe9, Leu40, and Val54. The conformation of all side chains except for Phe9 are the same in uncomplexed and complexed enzyme; the side chain of Phe9, however, must swing away from the pocket in the complexed enzyme in order to accommodate the Phe219 side chain). The stability of helix9 in the F219W mutant is most likely compromised due to the presence of a bulkier indole side chain which is not tolerated well at the packing interface at this position thus resulting in a disfunctional enzyme. Loss of conformational entropy of the larger indole side chain upon helix formation probably does not account for the destabilization of helix9 in the F219W mutant. Furthermore, since a tryptophan at position 219 is located at the hydrophobic face of the amphipathic helix, destabilization of helix9 in the F219W mutant should not be due to a drive to segregate Trp219 to the polar face of the helix. A looser packing of helix9 onto domain I could account for the low quantum yield and more polar environment observed for Trp219 (i.e., relative to Trp20). In a more loosely packed state, the side chains of Trp219 and Arg220 could be closer together resulting in quenching of the indole's fluorescence. A role for tertiary interactions between residues at position 219 and domain I in stabilizing helix9 has also been suggested in a study with rat GSTA1-1 (*20*). Replacement of Phe219 with either Ile or Leu enhanced pressure-induced conformational changes in helix9 whereas the introduction of a putative tertiary hydrogen bond between a Tyr at position 219 and Tyr8 enhanced the stability of helix9.

Active-Site Ligands Stabilize Helix9. We find that the urea-induced exposure of hydrophobic surface is reduced moderately by ethacrynic acid but strongly by glutathione or *p*-bromobenzylglutathione. Therefore, helix9 appears to be more tightly secured to the GST in its complex with *p*-bromobenzylglutathione and glutathione than with ethacrynic acid. This is supported by the extent of tertiary contacts between helix9 and protein (see above and Figure 8). There is no crystal structure available for the complex with glutathione to indicate the extent of tertiary interactions between helix9 and hGSTA1-1. However, according to our data with glutathione and *p*-bromobenzylglutathione, it seems highly likely that its interactions with helix9 are similar to those observed with *S*-bromobenzylglutathione. The lower stabilizing effect by ethacrynic acid might be explained by the absence of the two ion pair interactions (see above and Figure 8). Crystallographic data (*18*) suggests that the conformation of helix9 with bound ethacrynic is not as well-defined (i.e., it does not adopt a more stable position) than that for helix9 with *S*-benzylglutathione (*17*). These active-site ligands had no significant effect on the urea-dependent ANS-binding behavior of a9del mutant GSTA1-1.

ANS binding to wild-type GSTA1-1 reaches a maximum level at 4 M urea for uncomplexed and glutathione-complexed enzyme whereas the binding maximum is achieved at a higher (4.5 M) urea concentration for enzyme complexed with either ethacrynic acid or *p*-bromobenzylglutathione (Figure 5). These findings are consistent with the fluorescence unfolding transitions, which show that glutathione exerts little overall stabilizing effect while *p*-bromobenzylglutathione exerts a small stabilizing effect on the global structure of GSTA1-1 (Figure 4). Inspection of the crystal structures for uncomplexed and complexed hGSTA1-1 (*17*, *18*) indicates that there are no significant ligand-induced conformational changes in the structure from residue 1−206 including helix2 at the active site. Glutathione analogues have also been shown to stabilize class π GSTP1-1 (*42*). Despite the absence/presence of a ligand-induced global stabilization effect, the enzyme activity transitions are stabilized significantly against urea for hGSTA1-1 complexed with either glutathione or *p*-bromobenzylglutathione (i.e., the "pretransitions" are much less dependent upon urea when compared with those obtained for uncomplexed enzyme and the enzyme deactivation transitions are shifted to higher urea concentrations; Figure 4). These effects are most likely due to a ligand-induced stabilization of helix9. However, even for the complexed protein, their enzyme deactivation and fluorescence transitions do not coincide indicating the instability of helix9 at the higher concentrations of urea. Noncoincident activity (functional) and fluorescence (structural) transitions have not been observed for class π (*11*, *12*) or class μ Sj26GST (*16*). These enzymes exhibit two-state unfolding/refolding behavior and are representatives of the same subunit interface-type group to which class α GSTs belong (*7*). While the multiple confomational states of helix9 in hGSTA1-1 are reduced when ligands occupy the active site, the mobility of helix9 is reduced most when both G- and H-sites are occupied simultaneously. Occupation of the G-site affords a slightly less stabilizing effect, while much lower stabilization of helix9 is observed when only the H-site is occupied.

Helix9 and Ligandin Function. In addition to its contribution toward catalytic function and protein dynamics, helix9 also appears to play a role in the binding of nonsubstrate ligands at two distinct ligandin sites. The binding affinity for the nonsubstrate ligands ANS and BSP is enhanced when helix9 is immobilized and stabilized by active-site ligands that occupy the G-site (i.e., glutathione and *p*-bromobenzylglutathione but not ethacrynic acid which occupies only a small portion of the G-site adjacent to the H-site) (Figure 6). The two dyes bind different sites on wild-type hGSTA1-1 (*24*, *25*, *31*); ANS binds a hydrophobic site at the subunit interface whereas BSP binds a site on each subunit which is located in close proximity to Trp20 (this study and ref *25*). The ANS-binding site is similar to the one to which estradiol disulfate and AEDANS bind (*9*, *25*) while the BSP-binding site is probably similar to one which 2-hydroxy-5-nitrobenzyl alcohol (*43*) binds. The BSP site in murine class α GST has also been shown to be distinct from the ANS site and to be in close proximity to Trp20 (*43*). Topographically, the sulfonate buffers Hepes and Mes bind a similar region in class π GSTP1-1 (*44*, *45*). Inhibition of GST activity by the binding of nonsubstrate compounds would be explained by the proximity of the active site to these nonsubstrate ligand-binding sites (*31*). When helix9 becomes immobilized as a consequence of the binding of active-site ligands, the C-terminal residue (Phe221) of the A1 polypeptide chain becomes located close to the cleft at the subunit interface (see Figure 1). It is possible that Phe221 contributes structurally toward the formation of a higher affinity nonsubstrate site at the dimer interface. In the complexes of hGSTA1-1 with active-site ligand (*17*, *18*), the side chain of Phe221 contacts the side chain of Val110 from domain II (Figure 8) and together they would form a hydrophobic wall for the binding site, thus increasing the hydrophobicity of the site in glutathione/analogue complexed GSTA1-1. Covalent labeling of the neighboring Cys111 has identified this region to be involved in binding nonsubstrate ligands (*25*, *26*). Although the overall ligand-induced conformational states appear to be similar irrespective of the type of active-site ligand, crystallographic data (*17*, *18*) indicate that the conformations of the C-terminus of helix9 and the side chain of Phe221 are different with *S*-bromobenzylglutathione and ethacrynic acid. These differences could be the basis for the inability of bound ethacrynic acid to enhance the binding of ANS. The structural basis for improved BSP binding by the ligand-induced stabilization of helix9 is not known at present. Disruption of helix9 by urea or its removal from GSTA1-1 (i.e., a9del) creates an additional hydrophobic site for ANS most likely the region on domain I against which the helix usually packs.

Dynamics of Helix9 and Protein Unfolding/Refolding. In light of the present data, the two-state equilibrium unfolding/refolding model proposed earlier for hGSTA1-1 (*9*) can be modified to a four-state model in order to accommodate the dynamics of helix9:

$$N_2(\text{helix9stable}) \leftrightarrow N_2(\text{helix9mobile}) \leftrightarrow N_2(\text{helix9"coil"}) \leftrightarrow 2U$$

where U is the unfolded monomer. N_2(helix9stable) is native folded hGSTA1-1 in the presence of bound active-site ligand and represents the fully active conformational state of the enzyme. The ligand-induced stabilization of helix9 reduces solvent-accessible hydrophobic surface on domain I by

facilitating firmer packing at the hydrophobic interface between helix and GST. Although helix9 is not a primary structural determinant for sequestering glutathione at the G-site, the presence of the thiol at the G-site reduces helix9 mobility and facilitates its stability. The above-average temperature factors for helix9 in enzyme-ligand binary complexes (*17*, *18*) indicates that the helix structure is not completely rigid but is flexible. Slightly different conformations have been observed for helix9 in complexes with different ligands, attesting to its flexibility thus enabling the active site to accommodate structurally diverse electrophilic substrates. Furthermore, the affinity for nonsubstrate ligands bound at "ligandin" sites is enhanced when helix9 is stabilized. The C-terminus region (including helix9) of the class α polypeptide, therefore, appears not to have been optimized for stability but rather for catalytic and ligandin function. Considering the high concentration of reduced glutathione in human cells (up to 10 mM), hGSTA1-1 is most likely sequestered by glutathione and exists in a physiological N_2(helix9stable) form. This could also protect the GSTA1-1 molecule from proteolytic attack at the C-terminus. This region in rat GSTA1-1 has been shown to be susceptible to proteolysis (*20*). N_2(helix9mobile) represents native folded hGSTA1-1 in the absence of active-site ligand in which the helix is more loosely packed against the protein but does not swing away into bulk solvent. The closure of helix9 over domain I (even loosely bound) would reduce the amount of surface accessible to solvent. Charge−helix dipole and side-chain ion pair interactions within the helix could increase the stability of helix9 but its sequence nevertheless demonstrates an unfavorable tendency to form a helix. It is possible that tertiary nonpolar interactions on the hydrophobic face of the amphipathic helix contribute sufficient stability to populate the helix on the surface of domain I despite the low helix propensity. The existence of a mixed population of helical and partial helical (e.g., frayed C-terminus) conformers cannot be excluded. The mobility of helix9 would make it more susceptible to urea-induced structural changes than a helix9 which is stabilized by active-site ligands. N_2(helix9mobile) displays a lower affinity for nonsubstrate ligands bound at the ligandin sites. N_2-(helix9"coil") is hGSTA1-1 with the sequence for helix9 displaying substantial nonhelicity. The tertiary hydrophobic interactions which stabilize/immobilize helix9 onto the GST are disrupted by denaturant resulting in diminished packing at the helix−protein interface. The reduction of tertiary interactions most likely results in an increased population of partial helix and nonhelical structures leading to a marked impairment in catalytic function. The structural changes associated with this are accompanied by an increased exposure of hydrophobic surface and Trp20 to solvent. It appears highly unlikely that helix9 is an independent folding unit in the absence of tertiary interactions.

Furthermore, we find that the deletion of the C-terminus of hGSTA1-1 simplifies the protein's unfolding kinetics from a three-state pathway (*9*, *10*):

$$N_2 \rightarrow N_2^* \rightarrow 2U$$

to a two-state pathway

$$N_2^{\#} \rightarrow 2U$$

N_2 is native hGSTA1-1 uncomplexed with active-site ligand; i.e., the N_2(helix9mobile) form referred to above; N^*_2 is a transient dimeric intermediate rapidly formed as a result of structural changes at the domain-domain interface near Trp20; $N_2^{\#}$ is folded hGSTA1-1 without helix9; U is unfolded monomer. N^*_2 and $N_2^{\#}$ appear to share similar structural features according to their behavior/properties (e.g., enhanced Trp20 fluorescence). Their unfolding transition states occupy similar positions on the reaction coordinate diagram based on solvent accessibility. Helix9, therefore, does not impact on the kinetics of the global unfolding of the core structure of uncomplexed hGSTA1-1. The $N_2 \rightarrow N^*_2$ transition observed for wild-type enzyme appears to be the consequence of the destabilization/unfolding of helix9 which impacts on the tertiary environment of Trp20 at the domain-domain interface and which likely involves the C-terminus of helix8.

REFERENCES

1. Armstrong, R. N. (1997) *Chem. Res. Toxicol. 10*, 2−18.
2. Listowski, I. (1993) in *Hepatic transport and bile secretion: physiology and pathophysiology* (Tavoloni, N., and Berk, P., Eds.) pp 397−405, Raven Press, New York.
3. Mannervik, B., Alin, P., Guthenberg, C., Jenssen, H., Tahir, M. K., Warholm, M., and Jornvall, H. (1985) *Proc. Natl. Acad. Sci. U.S.A. 82*, 7202−7206.
4. Ji, X., von Rosenvinge, E. C. M., Johnson, W. W., Tomarev, S. I., Piatigorski, J., Armstrong, R. N., and Gilliland, G. L. (1995) *Biochemistry 34*, 5317−5328.
5. Meyer, D. J., Coles, B., Pemble, S. E., Gilmore, K. S., Fraser, G. M., and Ketterer, B. (1991) *Biochem. J. 274*, 409−414.
6. Pemble, S. E., Wardle, A. F., and Taylor, J. B. (1996) *Biochem. J. 319*, 749−754.
7. Dirr, H. W., Reinemer, P., and Huber, R. (1994) *Eur. J. Biochem. 220*, 645−661.
8. Wilce, M. C. J., and Parker, M. W. (1994) *Biochim. Biophys. Acta 1205*, 1−18.
9. Wallace, L. A., Sluis-Cremer, N., and Dirr, H. W. (1998) *Biochemistry 37*, 5320−5328.
10. Wallace, L. A., Blatch, G. L., and Dirr, H. W. (1998) *Biochem. J. 336*, 413−418.
11. Dirr, H. W., and Reinemer, P. (1991) *Biochem. Biophys. Res. Commun. 180*, 294−300.
12. Erhardt, J., and Dirr, H. W. (1995) *Eur. J. Biochem. 230*, 614−620.
13. Sluis-Cremer, N., and Dirr, H. (1995) *FEBS Lett. 371*, 94−98.
14. Sluis-Cremer, N., Naidoo, N., and Dirr, H. (1996) *Eur. J. Biochem. 242*, 301−307.
15. Stevens, J. M., Hornby, J. A. T., Armstrong, R. N., and Dirr, H. W. (1998) *Biochemistry 37*, 15534−15541.
16. Kaplan, W., Hüsler, P., Klump, H., Erhardt, J., Sluis-Cremer, N., and Dirr, H. W. (1997) *Protein Sci. 6*, 399−406.
17. Sinning, I., Kleywegt, G. J., Cowan, S. W., Reinemer, P., Dirr, H. W., Huber, R., Gilliland, G. L., Armstrong, R. N., Ji, X., Board, P. G., Olin, B., Mannervik, B., and Jones, T. A. (1993) *J. Mol. Biol. 232*, 192−212.
18. Cameron, A. D., Sinning, I., L'Hermite, G., Olin, B., Board, P. G., Mannervik, B., and Jones, T. A. (1995) *Structure 3*, 717−727.
19. Board, P. G., and Mannervik, B. (1991) *Biochem. J. 275*, 171−174.
20. Atkins, W. M., Dietze, E. C., and Ibarra, C. (1997) *Protein Sci. 6*, 873−881.
21. Lian, L.-Y., (1998) *Cell. Mol. Life Sci. 54*, 359−362.
22. McTique, M., Williams, D. R., and Tainer, J. A. (1995) *J. Mol. Biol. 246*, 21−27.
23. Ji, X., von Rosenvinge, E. C., Johnson, W. W., Armstrong, R. N., and Gilliland, G. L. (1996) *Proc. Natl. Acad. Sci. U.S.A. 93*, 8208−8213.

24. Sluis-Cremer, N., Naidoo, N. N., Kaplan, W. H., Manoharan, T. H., Fahl, W. E., and Dirr, H. W. (1996) *Eur. J. Biochem. 241*, 484−488.
25. Sluis-Cremer, N., Wallace, L., Burke, J., Stevens, J., and Dirr, H. (1998) *Eur. J. Biochem. 257*, 434−442.
26. Barycki, J. J. and Colman, R. F. (1997) *Arch. Biochem. Biophys. 345*, 16−31.
27. Stenberg, G., Bjornestedt, R., and Mannervik, B. (1992) *Protein Expression Purif. 3*, 80−84.
28. Weiner, M. P., Costa, G. L., Schoettlin, W., Cline, J., Mathur, E., and Bauer, J. C. (1994) *Gene 151*, 119−123.
29. Laemmli, U. K. (1970) *Nature* (*London*) *227*, 680−685.
30. Perkins, S. J. (1986) *Eur. J. Biochem. 157*, 169−180.
31. Bico, P., Erhardt, J., Kaplan, W., and Dirr, H. (1995) *Biochim. Biophys. Acta 1247*, 225−230.
32. Tonomura, B., Nakatani, H., Ohnishi, M., Yamaguchi-Ito, J., and Hiromi, K. (1978) *Anal. Biochem. 84*, 370−383.
33. Lacroix, E., Viguera, A. R., and Serrano, L. (1998) *J. Mol. Biol. 284*, 173−191.
34. Johnson, W. C., Jr. (1990) *Proteins: Struct. Funct. Gene. 7*, 205−214.
35. Myers, J. K., Pace, C. N., and Scholz, J. M. (1995) *Protein Sci. 4*, 2138−2148.
36. Semisotnov, G. V., Rodionova, N. A., Kutyshenko, V. P., Ebert, B., Blank, J., and Ptitsyn, O. B. (1987) *FEBS Lett. 224*, 9−13.
37. Kumar, T. K. S., Jayaraman, G., Lin, W.-Y., and Yu, C. (1996) *Biochim. Biophys. Acta 1294*, 103−105.
38. Tanford, C. (1970) *Adv. Protein Chem. 24*, 1−95.
39. Widersten, M., Bjornestedt, R., and Mannervik, B. (1996) *Biochemistry 35*, 7731−7742.
40. Wang, R. W., Nweton, D. J., Johnson, A. R., Pickett, C. B., and Lu, A. Y. H. (1993) *J. Biol. Chem. 268*, 23981−23985.
41. Chakrabartty, A., and Baldwin, R. L. (1995) *Adv. Protein Chem. 46*, 141−176.
42. Erhardt, J., and Dirr, H. W. (1996) *FEBS Lett. 391*, 313−316.
43. McCarthy, R. M., Farmer, P., and Sheenan, D. (1996) *Biochim. Biophys. Acta 1293*, 185−190.
44. Ji, X., Tordova, M., O'Donnell, R., Parsons, J. F., Hayden, J. B., Gilliland, G. L., and Zimniak, P. (1997) *Biochemistry 36*, 9690−9702.
45. Prade, L., Huber, R., Manoharan, T. H., Fahl, W. E., and Reuter, W. (1997) *Structure 5*, 1287−1295.
46. Kraulis, P. J. (1991) *J. Appl. Crystallogr. 24*, 946−950.
47. Matulis, D., Baumann, C. G., Bloomfield, V. A., and Lovrien, R. E. (1999) *Biopolymers 49*, 451−458.
48. Nieslanik, B. S., Dabrowski, M. J., Lyon, R. P., and Atkins, W. M. (1999) *Biochemistry 38*, 6971−6980.

BI991179X